

Simultaneous Color Holography

ERIC MARKLEY, Reality Labs Research, Meta
 NATHAN MATSUDA, Reality Labs Research, Meta
 FLORIAN SCHIFFERS, Reality Labs Research, Meta
 OLIVER COISSART, Reality Labs Research, Meta
 GRACE KUO, Reality Labs Research, Meta



Fig. 1. Simultaneous color holograms captured in experiment. Traditionally, color holograms are illuminated sequentially with a unique spatial light modulator (SLM) pattern for each color channel. In this work we outline a flexible framework that enables the use of a single SLM pattern for red-green-blue (RGB) holograms using simultaneous RGB illumination. We validate this framework experimentally on a simple and compact optical setup.

Computer generated holography has long been touted as the future of augmented and virtual reality (AR/VR) displays, but has yet to be realized in practice. Previous high-quality, color holographic displays have either made a 3 \times sacrifice on frame rate by using a sequential illumination scheme or have made use of multiple spatial light modulators (SLM) and/or bulky, complex optical setups. The reduced frame rate of sequential color introduces distracting judder and color fringing in the presence of head motion while the form factor of current simultaneous color systems is incompatible with a head-mounted display. In this work, we propose a framework for simultaneous color holography that allows the use of the full SLM frame rate while maintaining a compact and simple optical setup. State-of-the-art hologram quality is achieved through a perceptual loss function, a physics-based neural network wavefront propagator, and a camera-calibrated forward model. We measurably improve hologram quality compared to other simultaneous color methods and move one step closer to the realization of color holographic displays for AR/VR.

ACM Reference format:

Eric Markley, Nathan Matsuda, Florian Schiffers, Oliver Coissart, and Grace Kuo. 2023. Simultaneous Color Holography. 1, 1, Article 1 (March 2023), 20 pages.

<https://doi.org/10.1145/nnnnnnnn.nnnnnnn>

1 INTRODUCTION

Holographic displays are a promising technology for augmented and virtual reality (AR/VR). Such displays use a spatial light modulator (SLM) to shape an incoming coherent wavefront so that it appears as though the wavefront came from a real, three-dimensional (3D) object. The resulting image can have natural defocus cues, providing a path to resolve the vergence-accommodation conflict of stereoscopic displays [Kim et al. 2022b]. Additionally, the fine-grain control offered by holography can also correct for optical aberrations, provide custom eyeglass prescription correction in software, and enable compact form-factors [Maimone et al. 2017], while improving light

efficiency compared traditional LCD or OLED displays [Yin et al. 2022]. Recent publications have demonstrated significant improvement in hologram image quality [Choi et al. 2021a; Maimone et al. 2017; Peng et al. 2020] and computation time [Eybposh et al. 2020; Shi et al. 2021], bringing holographic displays one step closer to practicality. However, color holography for AR/VR has remained an open problem.

Traditionally, red-green-blue (RGB) holograms are created through *field sequential color*, where a separate hologram is computed for each of the three wavelengths and displayed in sequence and synchronized with the color of the illumination source. Due to persistence of vision, this appears as a single full color image if the update is sufficiently fast, enabling color holography for static displays. However, in a head-mounted AR/VR system displaying world-locked content, framerate requirements are higher to prevent noticeable judder [Van Waveren 2016]. Furthermore, field sequential color can lead to visible spatial separation of the colors, particularly when the user rotates their head while tracking a fixed object with their eyes [Riecke et al. 2006]. Although these negative effects can be mitigated with high framerate displays, the most common SLM technology for holography, liquid-crystal-on-silicon (LCoS), is quite slow due to the physical response time of the liquid crystal (LC) layer [Zhang et al. 2014]. Although most commercial LCoS SLMs can be driven at 60 Hz, at that speed the SLM will have residual artifacts from the prior frames [Haist and Osten 2015]. Micro-electro-mechanical system (MEMS) SLMs can be much faster (in the kilohertz range) but so far have larger pixels and limited bit depth [Choi et al. 2022; Duerr et al. 2021].

In this work, we aim to display RGB holograms using only a single SLM pattern, enabling a 3 \times increase in framerate compared to sequential color and removing color fringing artifacts in the presence of head motion. Our compact setup does not use a physical

filter in the Fourier plane or bulky optics to combine color channels. Instead, the full SLM is simultaneously illuminated by an on-axis RGB source, and we optimize the SLM pattern to form the three color image. We design a flexible framework for end-to-end optimization of the digital SLM input from the target RGB intensity, allowing us to optimize for SLMs with extended phase range, and we develop a color-specific perceptual loss function which further improves color fidelity. Our method is validated experimentally on 2D and 3D content.

Specifically, we make the following contributions:

- We introduce a novel algorithm for generating simultaneous color holograms which takes advantage of the extended phase range of the SLM in an end-to-end manner and uses a new loss function based on human color perception.
- We analyze the “depth replicas” artifact in simultaneous color holography and demonstrate how these replicas can be mitigated with extended phase range.
- We demonstrate high quality experimental simultaneous color holograms in both 2D and 3D using a custom camera-calibrated model.

2 RELATED WORKS

Field Sequential Color. The vast majority of color holographic displays use field sequential color in which the SLM is sequentially illuminated by red, green, and blue sources while the SLM pattern is updated accordingly [Chakravarthula et al. 2022, 2019, 2020; Choi et al. 2021a,b; Jang et al. 2018; Li et al. 2016; Maimone et al. 2017; Peng et al. 2021, 2020; Shi et al. 2021; Yang et al. 2022]. Field sequential color is effective at producing full color holograms but reduces framerate by a factor of 3x. This is a challenge for LCoS SLMs where framerate is severely limited by the LC response time [Zhang et al. 2014]. Although, SLMs based on MEMS technology can run at high framerates in the kilohertz range [Duerr et al. 2021], so far these modulators are maximum 4-bit displays, with most being binary [Choi et al. 2022; Kim et al. 2022b; Lee et al. 2022]. Even with high framerate modulators, it may be worthwhile to maintain the full temporal bandwidth, since the extra bandwidth can be used to address other holography limitations. For example, speckle can be reduced through temporal averaging [Choi et al. 2022; Kim et al. 2022b; Lee et al. 2022], and limited etendue can be mitigated through pupil scanning [Jang et al. 2018; Kim et al. 2022a].

Spatial Multiplexing. An alternate approach is spatial multiplexing, which maintains the native SLM framerate by using different regions of the SLM for each color. Most prior works in this area use three separate SLMs and an array of optics to combine the wavefronts [Nakayama et al. 2010; Shiraki et al. 2009; Yaraş et al. 2009]. Although this method produces high quality holograms, the resulting systems are bulky, expensive, and require precise alignment, making them poorly suited for near-eye displays. Spatial multiplexing can also be implemented with a single SLM split into sub-regions [Makowski et al. 2011, 2009]; while less expensive, this approach still requires bulky combining optics and sacrifices space-bandwidth product (SBP), also known as etendue. Etendue is already

a limiting factor in holographic displays [Kuo et al. 2020], and further reduction is undesirable as it limits the range of viewing angles or display field-of-view.

Frequency Multiplexing. Rather than split the physical extent of the SLM into regions, frequency multiplexing assigns each color a different region in the frequency domain, and the colors are separated with a physical color filter at the Fourier plane of a 4f system [Lin et al. 2019; Lin and Kim 2017; Makowski et al. 2010]. A variation on this idea uses different angles of illumination for each color so that the physical filter in Fourier space is not color-specific [Xue et al. 2014]. Frequency multiplexing can also be implemented with white light illumination, which reduces speckle noise at the cost of resolution [Kozacki and Chlipala 2016; Yang et al. 2019]. However, all of these techniques involve filtering in Fourier space, which sacrifices system etendue and requires a bulky 4f system.

Depth Division and Bit Division for Simultaneous Color. The prior methods most closely related to our work also use simultaneous RGB illumination over the SLM, maintain the full SLM etendue, and don’t require a bulky 4f system [Pi et al. 2022]. We refer to the first method as *depth division multiplexing* which takes advantage of the ambiguity between color and propagation distance (explained in detail in Sec. 3.1) and assigns each color a different depth [Makowski et al. 2010, 2008]. After optimizing with a single color for the correct multiplane image, the authors show they can form a full color 2D hologram when illuminating in RGB. However, this approach does not account for wavelength dependence of the SLM response, and since it explicitly defines content at multiple planes, it translates poorly to 3D.

Another similar approach is *bit division multiplexing*, which takes advantage of the extended phase range of LCoS SLMs [Jesacher et al. 2014]. The authors calibrate an SLM lookup-table consisting of phase-value triplets (for RGB) as a function of digital SLM input, and they note that SLMs with extended phase range (up to 10π) can create substantial diversity in the calibrated phase triplets. After pre-optimizing a phase pattern for each color separately, the lookup-table is used on a per-pixel basis to find the digital input that best matches the desired phase for all colors. In our approach, we also use an extended SLM phase range for the same reason, but rather than using a two-step process, we directly optimize the output hologram. This flexible framework also allows us to incorporate a perceptual loss function to further improve perceived image quality.

Algorithms for Hologram Generation. Our work builds on a body of literature applying iterative optimization algorithms to holographic displays. Perhaps most popular is the Gerchberg-Saxton (GS) method [Gerchberg 1972], which is effective and easy to implement, but does not have an explicitly defined loss function, making it challenging to adapt to specific applications. Zhang et al. [2017] and Chakravarthula et al. [2019] were the first to explicitly formulate the hologram generation problem in an optimization framework. This framework has been very powerful, enabling custom loss functions [Choi et al. 2022] and flexible adaptation to new optical configurations [Choi et al. 2021b; Gopakumar et al. 2021]. In particular, perceptual loss functions can improve the perceived image by taking aspects of human vision into account, such as human visual

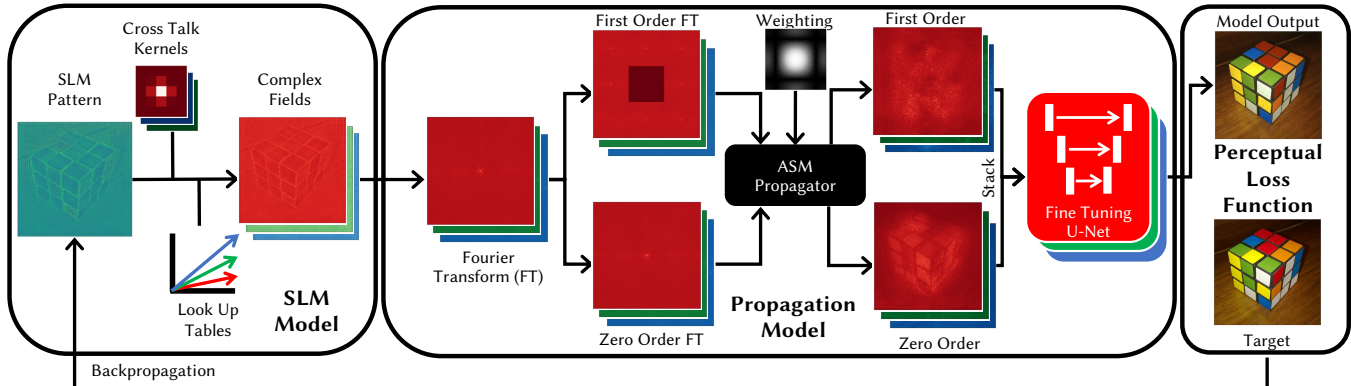


Fig. 2. Hologram optimization framework. This figure illustrates the three key components of the simultaneous color optimization framework: an SLM model, a propagation model, and a perceptual loss function. The SLM model maps voltage values to a complex field using a learned cross-talk kernel and a linear lookup table. The complex waveform from the SLM is then propagated to the sensor plane using a modified version of the model proposed by Gopakumar et al. [2021], which separates the zeroth and first diffraction orders and combines them through a U-Net. The output is then fed into the perceptual loss function, and gradients are calculated using Pytorch’s autograd implementation. The SLM voltages are then updated using these gradients. Rubik’s cube source image by Iwan Gabovitch (CC BY 2.0).

acuity [Kuo et al. 2020], foveated vision [Walton et al. 2022], and sensitivity to spatial frequencies during accommodation [Kim et al. 2022b]. Like these prior works, we use an optimization-based framework which we adapt to account for the wavelength-dependence of the SLM; this also enables our new perceptual loss function for color, which is based on visual acuity difference between chrominance and luminance channels.

Camera-Calibration of Holographic Displays. When the model used for hologram generation does not match the physical system, deviations cause artifacts in the experimental holograms. Recently, several papers have addressed this issue using measurements from a camera in the system for calibration. Peng et al. [2020] proposed using feedback from the camera to update the SLM pattern for a particular image; although a single image can be improved, it does not extend to new content. A more flexible approach uses pairs of SLM patterns and camera captures to estimate the learnable parameters in a model, which is then used for offline hologram generation. Learnable parameters can be physically-based [Chakrabarti 2016; Kavakli et al. 2022; Peng et al. 2020], black box CNNs [Choi et al. 2021a], or a combination of both [Choi et al. 2022]. The choice of learnable parameters effects the ability of the model to match the physical system; we introduce a new parameter for modeling SLM cross talk and tailor the CNN architecture for higher diffraction orders from the SLM.

3 SIMULTANEOUS COLOR HOLOGRAPHY

A holographic image is created by a spatially coherent illumination source incident on an SLM. The SLM imparts a phase delay on the electric field; after light propagates some distance, the intensity of the electric field forms an image. Our goal in this work is to compute a single SLM pattern that simultaneously creates a three color RGB hologram. For instance, when the SLM is illuminated with a red source, the SLM forms a hologram of the red channel of an image;

with a green source the same SLM pattern forms the green channel; and with the blue source it creates the blue channel.

We propose a flexible optimization-based framework (Fig. 2) for generating simultaneous color holograms. We start with a generic model for estimating the hologram from the digital SLM pattern, s , as a function of illumination wavelength, λ :

$$g_\lambda = e^{i\phi_\lambda(s)} \quad (1)$$

$$I_{z,\lambda} = |f_{\text{prop}}(g_\lambda, z, \lambda)|^2. \quad (2)$$

Here, ϕ_λ is a wavelength-dependent function that converts the 8 bit digital SLM pattern to a phase delay, g_λ is the electric field coming off the SLM, f_{prop} represents propagation of the electric field, and $I_{z,\lambda}$ is the intensity a distance z from the SLM.

To calculate the SLM pattern, s , we can solve the following optimization problem

$$\underset{s}{\operatorname{argmin}} \sum_z \mathcal{L}(\hat{I}_{z,\lambda_r}, I_{z,\lambda_r}) + \mathcal{L}(\hat{I}_{z,\lambda_g}, I_{z,\lambda_g}) + \mathcal{L}(\hat{I}_{z,\lambda_b}, I_{z,\lambda_b}), \quad (3)$$

where \hat{I} is the target image, \mathcal{L} is a pixel-wise loss function such as mean-square error, and $\lambda_r, \lambda_g, \lambda_b$ are the wavelengths corresponding to red, green, and blue respectively. Since the model is differentiable, we solve Eq. 3 with gradient descent.

3.1 Color-Depth Ambiguity

A common model for propagating electric fields is Fresnel propagation¹ [Goodman 2005], which can be written in Fourier space as

$$f_{\text{fresnel}}(g, z, \lambda) = \mathcal{F}^{-1}\{\mathcal{F}\{g\} \cdot H(z, \lambda)\} \quad (4)$$

$$H(z, \lambda) = \exp\left(i\pi\lambda z\left(f_x^2 + f_y^2\right)\right) \quad (5)$$

¹Fresnel propagation is the paraxial approximation to the popular angular spectrum method (ASM). Since most commercial SLMs have pixel pitch greater than 3 μm , resulting in a maximum diffraction angle under 5° (well within the small angle approximation), Fresnel and ASM are almost identical for holography.

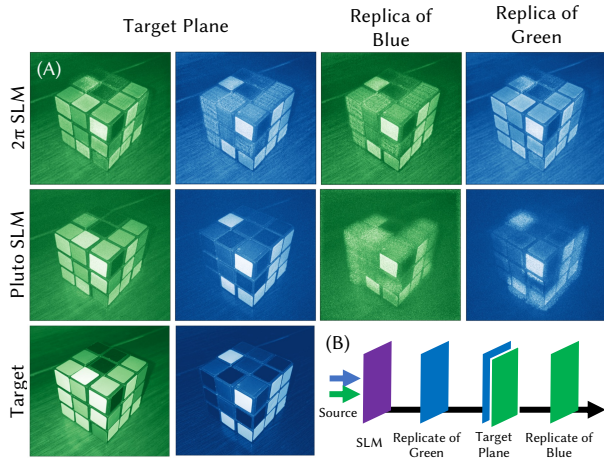


Fig. 3. Extended phase range reduces depth replicas in simulation. (A) Using an SLM with a uniform 2π phase range across all channels leads to strong depth replicas (top row), which reduce image quality at the target plane compared to the target (bottom row) and add in-focus content at depths that should be defocused. By using the extended phase Holoeye Pluto-2.1-Vis-016 SLM (with Red: 2.4π , Green: 5.9π , Blue: 7.4π phase ranges), depth replicas are significantly reduced (middle row), improving the quality of target plane holograms and creating defocused content at other depths. (B) Schematic illustrating the positions of the replicate planes and target plane. Note, this simulation was generated using RGB images and three color channels, but only the green and blue channels are displayed for clarity. (Rubik's cube source image by Iwan Gabovitch (CC BY 2.0).

where \mathcal{F} is a 2D Fourier transform, H is the Fresnel propagation kernel, and f_x, f_y are the spatial frequency coordinates. In Eq. 5, note that λ and z appear together, creating an ambiguity between wavelength and propagation distance.

To see how this ambiguity affects color holograms, consider the case where ϕ_λ in Eq. 1 is independent of wavelength ($\phi_\lambda = \phi$). For example, this would be the case if the SLM had a linear phase range from 0 to 2π at every wavelength. Although this is unrealistic for most off-the-shelf SLMs, it is a useful thought experiment. Note that if ϕ is wavelength-independent, then so is the electric field off the SLM ($g_\lambda = g$). In this scenario, assuming $f_{\text{prop}} = f_{\text{fresnel}}$, the Fresnel kernel is the only part of the model affected by wavelength.

Now assume that the SLM forms an image at distance z_0 under red illumination. From the ambiguity in the Fresnel kernel, we have the following equivalence:

$$H(z_0, \lambda_r) = H\left(\frac{\lambda_g}{\lambda_r} z_0, \lambda_g\right) = H\left(\frac{\lambda_b}{\lambda_r} z_0, \lambda_b\right). \quad (6)$$

This means the *same* image formed in red at z_0 will also appear at $z = z_0 \lambda_g / \lambda_r$ when the SLM is illuminated with green and at $z = z_0 \lambda_b / \lambda_r$ when the SLM is illuminated with blue. We refer to these additional copies as “depth replicas,” and this phenomena is depicted in Fig. 3. Note that depth replicas do not appear in sequential color holography, since the SLM pattern optimized for red is never illuminated with the other wavelengths.

If we only care about the hologram at the target plane z_0 , then the depth replicas are not an issue, and in fact, we can take advantage of

the situation for hologram generation: The SLM pattern for an RGB hologram at z_0 is equivalent to the pattern that generates a three-plane red hologram where the RGB channels of the target are each at a different depth ($z_0, z_0 \lambda_r / \lambda_g$, and $z_0 \lambda_r / \lambda_b$ for RGB respectively). This is the basis of the depth division multiplexing approach of Makowski et al. [2010, 2008], where the authors optimize for this three-plane hologram in red, then illuminate in RGB. Although this makes the assumption that ϕ does not depend on λ , this connection between simultaneous color and multi-plane holography suggests simultaneous color should be possible for a single plane, since multi-plane holography has been successfully demonstrated in prior work.

However, the ultimate goal of holography is to create 3D imagery, and the depth replicas could prevent us from placing content arbitrarily over the 3D volume. In addition, in-focus images can appear at depths that should be out-of-focus, which may prevent the hologram from successfully driving accommodation [Kim et al. 2022b]. We propose taking advantage of SLMs with extended phase range to mitigate the effects of depth replicas.

3.2 SLM Extended Phase Range

In general, the phase ϕ_λ of the light depends on its wavelength, which was not considered in Sec. 3.1. Perhaps the most popular SLM technology today is LCoS, in which rotation of birefringent LC molecules causes a change in refractive index. The phase of light traveling through the LC layer is delayed by

$$\phi_\lambda = \frac{2\pi d}{\lambda} n(s, \lambda), \quad (7)$$

where d is the thickness of the LC layer, and its refractive index, n , is controlled with the digital input s . n also depends on λ due to dispersion [Jesacher et al. 2014]. The wavelength dependence of ϕ_λ presents an opportunity to reduce or remove the depth replicas. Even if the propagation kernel H is the same for several (λ, z) pairs, if the phase, and therefore the electric field off the SLM, changes with λ , then the output image intensity at the replica plane will also be different. As the wavelength-dependence of ϕ_λ increases, the replicas are diminished.

We can quantify the degree of dependence on λ by looking at the derivative $d\phi/d\lambda$ which informs us that larger n will give λ more influence on the SLM phase. However, the final image intensity depends only on relative phase, not absolute phase; therefore, for the output image to have a stronger dependence on λ , we desire larger $\Delta n = n_{\text{max}} - n_{\text{min}}$. In addition, $d\phi/d\lambda$ increases with $-dn/d\lambda$, suggesting that more dispersion is helpful for simultaneous color. Although $d\phi/d\lambda$ also depends on the absolute value of λ , we have minimal control over this parameter since there are limited wavelengths corresponding to RGB. In summary, this means we can reduce depth replicas in simultaneous color with larger phase range on the SLM and higher dispersion.

However, there is a trade-off: As the range of phase increases, the limitations of the bit depth of the SLM become more noticeable, leading to increased quantization errors. We simulate the effect of quantization on hologram quality and find that PSNR and SSIM are almost constant for 6 bits and above. This suggests that each 2π range should have at least 6 bits of granularity. Therefore, we think that using a phase range of around 8π for an 8-bit SLM will

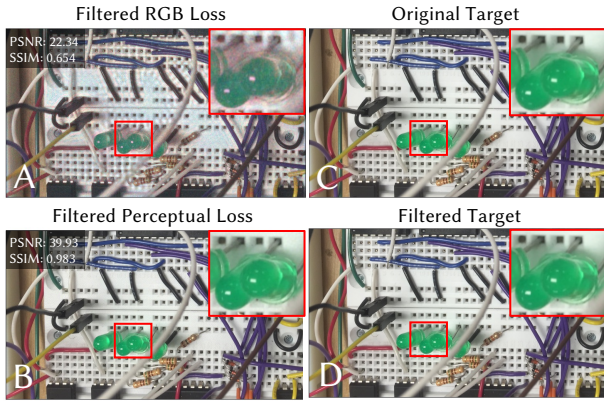


Fig. 4. Perceptual loss improves color fidelity and reduces noise in simulation. The first column of this figure depicts simulated holograms that were optimized with an RGB loss function (A) and our perceptual loss function (B). The same filters for the perceptual loss function then were applied to both of these simulated holograms as well as the target image. Image metrics were calculated between the filtered holograms and the filtered target image (D). All image metrics are better for the perceptually optimized hologram (B). One should also note that the filtered target (D) and original target (C) are indistinguishable suggesting our perceptual loss function only removes information imperceptible by the human visual system as intended.

be the best balance between replica reduction and maintaining accuracy for hologram generation. Figure 3 simulates the effect of extended phase range on depth replica removal. While holograms were calculated on full color images, only two color channels are shown for simplicity.

In the first row of Fig. 3, we simulate an SLM with no wavelength dependence to ϕ (i.e. $0 - 2\pi$ phase range for each color). Consequently, perfect copies appear at the replica planes. In the second row, we simulate using the specifications from an extended phase range SLM (Holoeye Pluto-2.1-Vis-016), which has 2.4π range in red, 5.9π range in green, and 7.4π range in blue demonstrating that replicas are substantially diminished with an extended phase range. By reducing the depth replicas, the amount of high frequency out of focus light at the sensor plane is reduced leading to improved hologram quality.

3.3 Perceptual Loss Function

Creating an RGB hologram with a single SLM pattern is an over-determined problem as there are $3\times$ more output pixels than degrees of freedom of the SLM. As a result, it may not be possible to exactly match the full RGB image, which can result in color deviations and de-saturation. To address this, we take advantage of color perception in human vision. There's evidence that the human visual system converts RGB images into a luminance channel (a grayscale image) and two chrominance channels, which contain information about the color [Wandell 1995]. The visual system is only sensitive to high resolution features in the luminance channel, so the chrominance channels can be lower resolution with minimal impact on the perceived image [Wandell 1995]. This observation is used in JPEG

compression [Pennebaker and Mitchell 1992] and subpixel rendering [Platt 2000], but to our knowledge, it has never been applied to holographic displays. By allowing the unperceived high frequency chrominance and extremely high frequency luminance features to be unconstrained, we can better use the the degrees of freedom on the SLM to faithfully represent the rest of the image.

Our flexible optimization framework allows us to easily change the RGB loss function in Eq. 3 to a perceptual loss. For each depth, we transform the RGB intensities of both \hat{I} (the target image) and I (the simulated image from the SLM) into opponent color space as follows:

$$\begin{aligned} O_1 &= 0.299 \cdot I_{\lambda_r} + 0.587 \cdot I_{\lambda_g} + 0.114 \cdot I_{\lambda_b} \\ O_2 &= I_{\lambda_r} - I_{\lambda_g} \\ O_3 &= I_{\lambda_b} - I_{\lambda_r} - I_{\lambda_g} \end{aligned} \quad (8)$$

where O_1 is the luminance channel, and O_2 , O_3 are the red-green and blue-yellow chrominance channels, respectively. We can then update Eq. 3 to

$$\operatorname{argmin}_s \sum_z \left[\mathcal{L} \left(\hat{O}_1 * k_1, O_1 * k_1 \right) + \mathcal{L} \left(\hat{O}_2 * k_2, O_2 * k_2 \right) + \mathcal{L} \left(\hat{O}_3 * k_3, O_3 * k_3 \right) \right], \quad (9)$$

where $*$ represents a 2D convolution with a low pass filter ($k_1 \dots k_3$) for each channel in opponent color space. \hat{O}_i and O_i are the i -th channel in opponent color space of \hat{I} and I , respectively. In order to mimic the contrast sensitivity functions of the human visual system, we implement filters in the Fourier domain by applying a low-pass filter of 45% of the width of Fourier space to the chrominance channels (O_2 , O_3) and a filter of 75% of the width of Fourier space to the luminance channel (O_1). These filter widths were heuristically determined.

By de-prioritizing high frequencies in chrominance and extremely high frequencies in luminance, the optimizer is able to better match the low frequency color. This low frequency color is what is perceptible by the human visual system. Figure 4 depicts the hologram quality improvement by optimizing with our perceptual loss function.

The first column of Fig. 4 shows the perceptually filtered versions of simulated holograms generated using an RGB loss function (Fig 4A) and our perceptual loss function (Fig 4B). The second column displays the original target image (Fig 4C) and the perceptually filtered target image (Fig 4D). It can be observed that the two targets are indistinguishable, indicating that our perceptual filter choices align well with the human visual system. The PSNR and SSIM values are higher for the perceptually optimized hologram, and it also appears less noisy and with better color fidelity. This suggests that the loss function has effectively shifted most of the error into imperceptible regions of the opponent color space. We see an average PSNR increase of 6.4 dB and average increase of 0.266 in SSIM across a test set of 294 images.

3.4 Simulation Comparisons

In Figure 5 we compare the performance of our method to the depth and bit division approach to simultaneous color holography. Depth



Fig. 5. **Comparison of bit division, depth division and our method of simultaneous color holography in simulation.** Bit division (Col. 1) is noisier than our method but achieves comparable color fidelity, although more washed out. The depth division method (Col. 2) is also noisier than our method and has inferior color fidelity. Our method matches the target image well. Our method uses our perceptual loss function and a high order angular spectrum propagation model with no learned components. Further implementation details for each method are available in the supplement.

and bit division use only a single SLM, make use of the full space-time-bandwidth product of the SLM, and contain no bulky optics or filters making these methods the most similar to our method. The holograms simulated with depth and bit division are much noisier and have lower color fidelity than our proposed method. The depth division simulated hologram has the worst color fidelity due to the replica planes discussed in Sec. 3.1 contributing defocused light at the target plane. Our method uses a perceptual loss function and the HOASM outlined by Gopakumar et al. [2021] to directly optimize the simultaneous color hologram, while comparison methods optimize indirectly. This direct approach produces less noisy holograms with better color fidelity.

4 CAMERA-CALIBRATED MODEL

We've demonstrated that our algorithm can generate simultaneous color holograms in simulation. However, experimental holograms frequently do not match the quality of simulations due to mismatch between the physical system and the model used in optimization (Eqs. 1, 2). Therefore, to demonstrate simultaneous color experimentally, we need to calibrate the model to the experimental system.

To do this, we design a model based on our understanding of the system's physics, but we include several learnable parameters representing unknown elements. To fit the parameters, we capture a dataset of SLM patterns and camera captures and use gradient descent to estimate the learnable parameters based on the dataset. Next we explain the model which is summarized in Fig. 2.

4.1 Learnable Parameters for Offline Calibration

Lookup Table. A key element in our optimization is ϕ_λ which converts the digital SLM input into the phase coming off the SLM, and it's important that this function accurately matches the behavior of the real SLM. Many commercial SLMs ship with a lookup-table (LUT) describing ϕ_λ ; however, the manufacturer LUT is generally only calibrated at a few discrete wavelengths. These wavelengths may not be accurate for the source used in the experiment. Therefore,

we learn a LUT for each color channel as part of the model. Based on a pre-calibration of the LUT using the approach of Yang et al. [2015], we observe the LUT is close to linear; we therefore parameterize the LUT with a linear model to encourage physically realistic solutions.

SLM Crosstalk. SLMs are usually modeled as having a constant phase over each pixel with sharp transitions at boundaries. However, in LCoS SLMs, elastic forces in the LC layer prevent sudden spatial variations, and the electric field that drives the pixels changes gradually over space. As a result, LCoS SLMs suffer from crosstalk, also called field-fringing, in which the phase is blurred [Apter et al. 2004; Moser et al. 2019; Persson et al. 2012]. We model crosstalk with a convolution on the SLM phase. Combined with our linear LUT described above, we can describe the phase off the SLM as

$$\phi_\lambda(s) = k_{\text{xt}} * (a_1 \cdot s + a_2) \quad (10)$$

where a_1, a_2 are the learn parameters of the LUT, and k_{xt} is a learned 5×5 convolution kernel representing crosstalk. Separate values of these parameters are learned for each color channel.

Propagation with Higher Diffraction Orders. The discrete pixel structure on the SLM creates higher diffraction orders that are not modeled well with ASM or Fresnel propagation. A physical aperture at the Fourier plane of the SLM can be used to block higher orders. However, accessing the Fourier plane requires a $4f$ system, which adds significant size to the optical system, reducing the practicality for head-mounted displays. Therefore, we chose to avoid additional lenses after the SLM and instead account for higher orders in the propagation model.

We adapt the higher-order angular spectrum model (HOASM) of Gopakumar et al. [2021].

The zero order diffraction, $G(f_x, f_y)$, and first order diffraction, $G_{1\text{st}}$ order, patterns are propagated with ASM to the plane of interest independently. Then the propagated fields are stacked and passed into a U-net, which combines the zero and first orders and returns

the image intensity:

$$f_{\text{ASM}}(G, z) = \mathcal{F}^{-1} \{G \cdot H_{\text{ASM}}(z)\} \quad (11)$$

$$I_z = \text{Unet}(f_{\text{ASM}}(G, z), f_{\text{ASM}}(G_{\text{1st order}}, z)), \quad (12)$$

where $H_{\text{ASM}}(z)$ is the ASM kernel. The U-Net architecture is detailed in the supplement; a separate U-net for each color is learned from the data. The U-Net helps to address any unmodeled aspects of the system that may affect the final hologram quality such as source polarization, SLM curvature, and beam profiles, and the U-net better models superposition of higher orders, allowing for more accurate compensation in SLM pattern optimization. Figure 8 compares ASM, HOASM, and our modified version with the U-Net.

5 IMPLEMENTATION

Experimental Setup. Our system starts with a fiber coupled RGB source, collimated with a 400 mm lens. The beam is aligned using two mirrors, passes through a linear polarizer and beamsplitter, reflects off the SLM (Holoeye-2.1-Vis-016), and passes through the beamsplitter a second time before directly hitting the color camera sensor with Bayer filter (FLIR GS3-U3-123S6C). As seen in Fig. 9, there's no bulky 4f system between the SLM and camera sensor, which allows the setup to be compact, but requires modeling of higher diffraction orders. The camera sensor is on a linear motion stage, enabling a range of propagation distances from $z = 80$ mm to $z = 130$ mm.

For our source, we use a superluminescent light emitting diode (SLED, Exalos EXC250011-00) rather than a laser due to its lower coherence, which has been demonstrated to reduce speckle in holographic displays [Deng and Chu 2017]. Although previous work showed state-of-the-art image quality by modeling the larger bandwidth of the SLED as a summation of coherent sources [Peng et al. 2021], we found the computational cost to be prohibitively high for our application due to GPU memory constraints. We achieved sufficient image quality while assuming a fully coherent model, potentially due to the U-net which is capable of simulating the additional blur we expect from a partially coherent source.

Calibration Procedure. We fit the learned parameters in our model (Eqs. 10 - 12) using a dataset captured on the experimental system. We pre-calculate 882 SLM patterns from a personally collected dataset of images using a naive ASM propagation model. Each SLM pattern is captured in 5 mm increments from $z = 90$ mm to 120 mm, resulting in a total of 6174 paired entries. The raw camera data is debayered and an affine transform is applied to align the image with the SLM (see Supplement for details). Model fitting is implemented in Pytorch using an L1 loss function between the model output and camera capture. To account for the camera color balance, we additionally learn a 3×3 color calibration matrix from the RGB simulated intensities to the captured color image. We train until convergence, which is typically reached between 50 and 100 epochs (2-3 days on Nvidia A6000 GPU).

Hologram Generation. After training, we can generate holograms by solving Eq. 9 using the trained model for $I_{z,\lambda}$, implemented with Pytorch's native auto-differentiation. The SLM pattern, s , is constrained to the range where the LUT is valid (for example, 0 - 255); the values outside that range are wrapped after every optimization

step. On the Nvidia A6000 GPU, it takes about two minutes to optimize a 2D hologram. Computation time for the optimization of a 3D hologram scales proportional to the number of depth planes.

6 EXPERIMENTAL RESULTS

2-Dimensional Holograms. We validate our simulation results by capturing holograms in experiment. The SLM patterns were optimized for a propagation distance of 120 mm using our perceptual loss function laid out in Section 3.3. A white border was added to each target image to improve the color fidelity by encouraging a proper white balance. After each hologram is captured, debayering is performed and a homography is applied to map from camera space to SLM space. The homography also downsamples the captured holograms to the same resolution as the SLM. The captured results are shown in Figure 6. The images match simulation well, validating our simultaneous color algorithm, although experimental results are noisier with lower color fidelity due to model-mismatch.

3-Dimensional Holograms. As mentioned earlier a major appeal of holography is the ability to solve the vergence-accommodation conflict without the need for eye tracking. Consequently, we also validate our method for 3D scenes. A 4-plane focal stack was rendered with 0.5 pixels blur radius per millimeter depth. Holograms were captured at distance from 90 mm to 120 mm in 10 mm increments. The results are displayed in Fig. 7, and quality is similar to the 2D case. These experimental results demonstrate the ability to form 3D color holograms with natural defocus blur from a single SLM frame.

7 LIMITATIONS

While our method improves hologram quality for simultaneous illumination and is compatible with VR and AR displays, it does have limitations. First, our method is not equally effective for all images. Natural images with high levels of texture work best, as they have similarly structured color channels and contain high frequency color information that is perceptually suppressible by our loss function. However, images with large flat areas may show noticeable artifacts such as the cat paws image in Figure 6. Unnatural images often have more saturated color, creating the more difficult task of finding an SLM pattern that can produce three largely unique holograms.

Additionally, our method takes on the order of minutes to calculate a single SLM pattern for a 2D image using a Nvidia A6000. This is incompatible with real time displays. Recent work has shown that neural nets can produce SLM patterns for holography in near real time while maintaining hologram quality [Eybposh et al. 2020; Shi et al. 2021; Yang et al. 2022]. A neural SLM pattern generator for simultaneous color holography is likely feasible, but has been left for future work.

8 CONCLUSION

In summary, we have developed a comprehensive framework for generating high-quality color holograms using simultaneous RGB illumination and a simple, compact optical setup. Our framework features a camera-calibrated, differentiable forward model that reduces model mismatch and allows for the use of custom loss functions.

By employing a perceptual loss function, we have successfully addressed the difficult challenge of simultaneous color holography, as validated by experimental testing in 2D and 3D. Our work brings us closer to creating holographic near-eye displays.

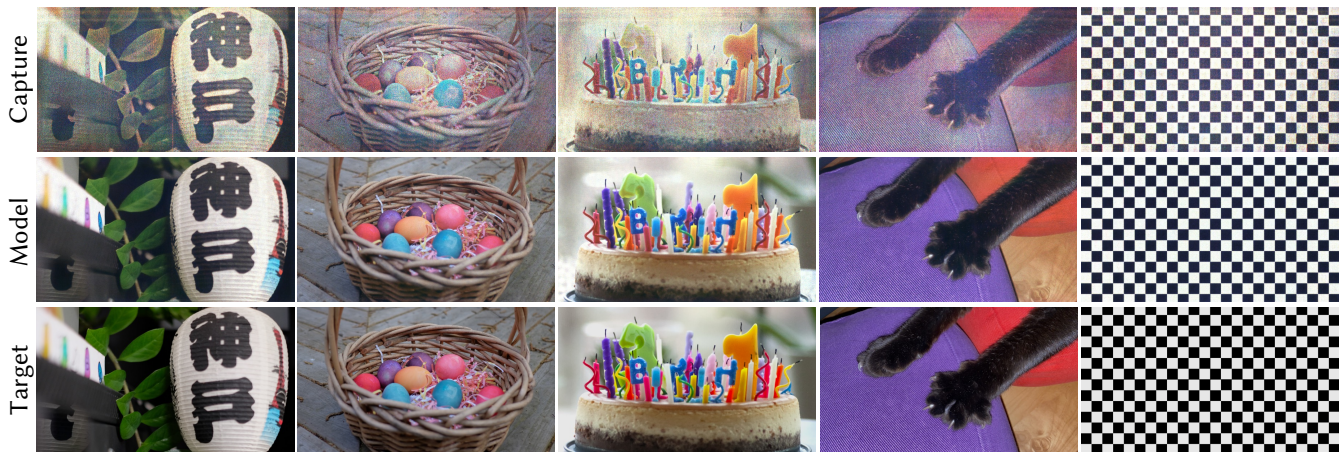


Fig. 6. Experimentally captured 2D holograms. This figure depicts experimentally captured holograms at a depth of 120 mm. Row one contains the experimentally captured images. Row two is the simulation output of the optimized SLM pattern. Row three contains the target images. While most of the captured holograms have good color fidelity, our method is least effective on highly saturated images with low texture, such as the cat paws in column 4, which represents a limitation of our method (see Sec. 7).



Fig. 7. Experimentally captured focal stack. This figure depicts a focal stack captured from 90 mm to 120 mm in 10 mm increments. Row one contains the experimentally captured images. Row two is the simulation output of the optimized SLM pattern. Row three contains the target images.

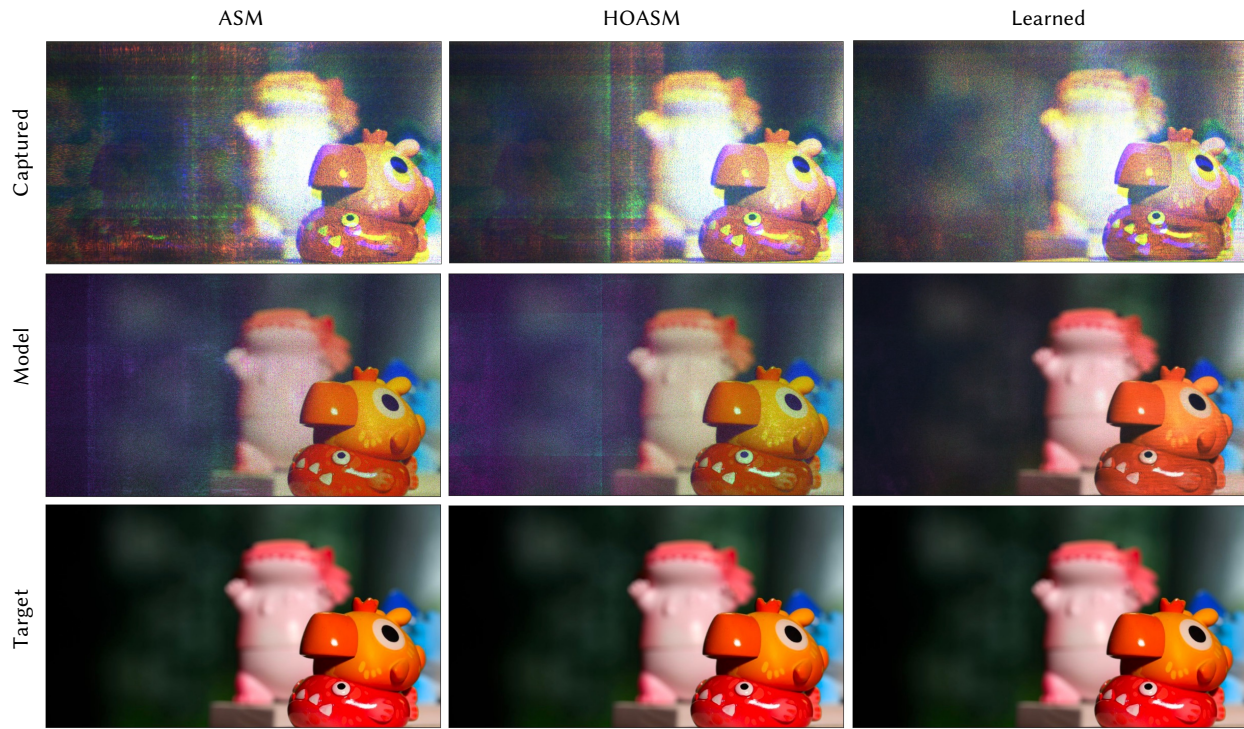


Fig. 8. Comparison of different propagation methods for suppressing higher diffraction orders. The first column shows the results obtained using the traditional angular spectrum method (ASM) which doesn't model higher diffraction orders. The second column shows the results obtained using HOASM which reduces the visibility of higher orders but fails to completely suppress them. The third column shows the results obtained using our proposed learned propagation method that includes a U-net, which largely suppresses the higher diffraction orders and results in a hologram with the fewest artifacts, suggesting the learned propagation model best matches the physical propagation.

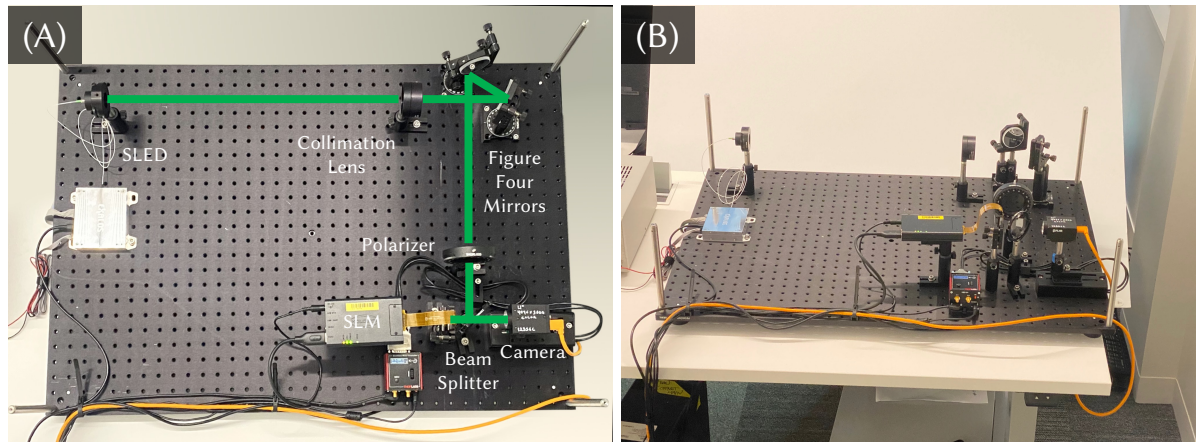


Fig. 9. Experimental setup. (A) Top view of our system with labeled components and approximate beam path is drawn in green. (B) Side-view of the system.

REFERENCES

- Boris Apté, Uzi Efron, and Eldad Bahat-Treidel. 2004. On the fringing-field effect in liquid-crystal beam-steering devices. *Applied optics* 43, 1 (2004), 11–19.
- Ayan Chakrabarti. 2016. Learning sensor multiplexing design through back-propagation. *Advances in Neural Information Processing Systems Nips* (2016), 3089–3097.
- Praneeth Chakravarthula, Seung-Hwan Baek, Ethan Tseng, Andrew Maimone, Grace Kuo, Florian Schiffers, Nathan Matsuda, Oliver Cossairt, Douglas Lamman, and Felix Heide. 2022. Pupil-aware Holography. *arXiv preprint arXiv:2203.14939* (2022).
- Praneeth Chakravarthula, Yifan Peng, Joel Kollin, Henry Fuchs, and Felix Heide. 2019. Wirtzinger holography for near-eye displays. *ACM Transactions on Graphics* 38, 6 (2019). <https://doi.org/10.1145/3355089.3356539>
- Praneeth Chakravarthula, Ethan Tseng, Tarun Srivastava, Henry Fuchs, and Felix Heide. 2020. Learned hardware-in-the-loop phase retrieval for holographic near-eye displays. *ACM Transactions on Graphics* 39, 6 (2020). <https://doi.org/10.1145/3414685.3417486>
- Suyeon Choi, Manu Gopakumar, Yifan Peng, Jonghyun Kim, Matthew O’Toole, and Gordon Wetzstein. 2022. Time-multiplexed Neural Holography: A Flexible Framework for Holographic Near-eye Displays with Fast Heavily-quantized Spatial Light Modulators. (2022), 1–9. <https://doi.org/10.1145/3522833.3530734>
- Suyeon Choi, Manu Gopakumar, Yifan Peng, Jonghyun Kim, and Gordon Wetzstein. 2021a. Neural 3D Holography: Learning Accurate Wave Propagation Models for 3D Holographic Virtual and Augmented Reality Displays. *ACM Transactions on Graphics* 40, 6 (2021). <https://doi.org/10.1145/3478513.3480542>
- Suyeon Choi, Jonghyun Kim, Yifan Peng, and Gordon Wetzstein. 2021b. Optimizing image quality for holographic near-eye displays with michelson holography. *Optica* 8, 2 (2021), 143–146.
- Yuanbo Deng and Daping Chu. 2017. Coherence properties of different light sources and their effect on the image sharpness and speckle of holographic displays. *Scientific Reports* 7, 1 (2017), 1–12. <https://doi.org/10.1038/s41598-017-06215-x>
- Peter Duerr, Andreas Neudert, Christoph Hohle, Hagen Stolle, Johannes Pleikies, and Hagen Sahm. 2021. MEMS Spatial Light Modulators for Real Holographic 3D Displays. In *MikroSystemTechnik Congress 2021; Congress*. 1–4.
- M Hosseini Ebyposh, Nicholas W Caira, Praneeth Chakravarthula, Mathew Atisa, and Nicolas C Pégard. 2020. High-speed computer-generated holography using convolutional neural networks. In *Optics and the Brain*. Optica Publishing Group, BTu2C–2.
- Ralph W Gerchberg. 1972. A practical algorithm for the determination of plane from image and diffraction pictures. *Optik* 35, 2 (1972), 237–246.
- Joseph W Goodman. 2005. *Introduction to Fourier optics*. Roberts & Company Publishers.
- Manu Gopakumar, Jonghyun Kim, Suyeon Choi, Yifan Peng, and Gordon Wetzstein. 2021. Unfiltered holography: optimizing high diffraction orders without optical filtering for compact holographic displays. *Optics Letters* 46, 23 (2021), 5822. <https://doi.org/10.1364/ol.442851>
- Tobias Haist and Wolfgang Osten. 2015. Holography using pixelated spatial light modulators—part 1: theory and basic considerations. *Journal of Micro/Nanolithography, MEMS, and MOEMS* 14, 4 (2015), 041310.
- Changwon Jang, Kiseung Bang, Gang Li, and Byoungcho Lee. 2018. Holographic near-eye display with expanded eye-box. *ACM Transactions on Graphics (TOG)* 37, 6 (2018), 1–14.
- Alexander Jesacher, Stefan Bernet, and Monika Ritsch-Marte. 2014. Colour hologram projection with an SLM by exploiting its full phase modulation range. *Optics Express* 22, 17 (8 2014), 20530. <https://doi.org/10.1364/oe.22.020530>
- Koray Kavaklı, Hakan Urey, and Kaan Akşit. 2022. Learned holographic light transport. *Applied Optics* 61, 5 (2022), B50–B55.
- Dongyeon Kim, Seung-Woo Nam, Byoungcho Lee, Jong-Mo Seo, and Byoungcho Lee. 2022b. Accommodative holography: improving accommodation response for perceptually realistic holographic displays. *ACM Transactions on Graphics (TOG)* 41, 4 (2022), 1–15.
- Jonghyun Kim, Manu Gopakumar, Suyeon Choi, Yifan Peng, Ward Lopes, and Gordon Wetzstein. 2022a. Holographic glasses for virtual reality. In *ACM SIGGRAPH 2022 Conference Proceedings*. 1–9.
- Tomasz Kozański and Maksymilian Chlipala. 2016. Color holographic display with white light LED source and single phase only SLM. *Optics Express* 24, 3 (feb 2016), 2189. <https://doi.org/10.1364/oe.24.002189>
- Grace Kuo, Laura Waller, Ren Ng, and Andrew Maimone. 2020. High resolution étendue expansion for holographic displays. *ACM Transactions on Graphics (TOG)* 39, 4 (2020), 66–1.
- Byoungcho Lee, Dongyeon Kim, Seungjae Lee, Chun Chen, and Byoungcho Lee. 2022. High-contrast, speckle-free, true 3D holography via binary CGH optimization. *Scientific reports* 12, 1 (2022), 1–12.
- Gang Li, Dukho Lee, Youngmo Jeong, Jaebum Cho, and Byoungcho Lee. 2016. Holographic display for see-through augmented reality using mirror-lens holographic optical element. *Optics letters* 41, 11 (2016), 2486–2489.
- Shu-Feng Lin, Hong-Kun Cao, and Eun-Soo Kim. 2019. Single SLM full-color holographic three-dimensional video display based on image and frequency-shift multiplexing. *Opt. Express* 27, 11 (may 2019), 15926–15942. <https://doi.org/10.1364/OE.27.015926>
- Shu-Feng Lin and Eun-Soo Kim. 2017. Single SLM full-color holographic 3-D display based on sampling and selective frequency-filtering methods. *Opt. Express* 25, 10 (may 2017), 11389–11404. <https://doi.org/10.1364/OE.25.011389>
- Andrew Maimone, Andreas Georgiou, and Joel S Kollin. 2017. Holographic near-eye displays for virtual and augmented reality. *ACM Transactions on Graphics (TOG)* 36, 4 (2017), 85.
- Michał Makowski, Izabela Ducin, Karol Kakarenko, Jarosław Suszak, Maciej Sypek, Andrzej Kolodziejczyk, P.-H Yao, C.-H Chen, J.-N 4 Kuo, and H.-W Wu. 2011. *Simple holographic projection in color*. Technical Report. 7–9 pages. www.osiris-project.eu
- Michał Makowski, Izabela Ducin, Maciej Sypek, Agnieszka Siemion, Andrzej Siemion, Jarosław Suszak, and Andrzej Kolodziejczyk. 2010. *Color image projection based on Fourier holograms*. Technical Report 8. 1227 pages.
- Michał Makowski, Maciej Sypek, Izabela Ducin, Agnieszka Fajst, Andrzej Siemion, Jarosław Suszak, and Andrzej Kolodziejczyk. 2009. Experimental evaluation of a full-color compact lensless holographic display. *Opt. Express* 17, 23 (2009), 20840–20846. <https://doi.org/10.1364/OE.17.020840>
- Michał Makowski, Maciej Sypek, and Andrzej Kolodziejczyk. 2008. *Colorful reconstructions from a thin multi-plane phase hologram*. Technical Report.
- Simon Moser, Monika Ritsch-Marte, and Gregor Thalhammer. 2019. Model-based compensation of pixel crosstalk in liquid crystal spatial light modulators. *Optics express* 27, 18 (2019), 25046–25063.
- Hirotaka Nakayama, Naoki Takada, Yasuyuki Ichihashi, Shin Awazu, Tomoyoshi Shimobaba, Nobuyuki Masuda, and Tomoyoshi Ito. 2010. *Real-time color electroholography using multiple graphics processing units and multiple high-definition liquid-crystal display panels*. Technical Report.
- Yifan Peng, Suyeon Choi, Jonghyun Kim, and Gordon Wetzstein. 2021. Speckle-free holography with partially coherent light sources and camera-in-the-loop calibration. *Science Advances* 7, 46 (2021). <https://doi.org/10.1126/sciadv.abg5040>
- Yifan Peng, Suyeon Choi, Nitish Padmanaban, and Gordon Wetzstein. 2020. Neural holography with camera-in-the-loop training. *ACM Transactions on Graphics* 39, 6 (11 2020). <https://doi.org/10.1145/3414685.3417802>
- William B Pennebaker and Joan L Mitchell. 1992. *JPEG: Still image data compression standard*. Springer Science & Business Media.
- Martin Persson, David Engström, and Mattias Goksör. 2012. Reducing the effect of pixel crosstalk in phase only spatial light modulators. *Optics express* 20, 20 (2012), 22334–22343.
- Dapu Pi, Juan Liu, and Yongtian Wang. 2022. Review of computer-generated hologram algorithms for color dynamic holographic three-dimensional display. <https://doi.org/10.1038/s41377-022-00916-3>
- John C Platt. 2000. Optimal filtering for patterned displays. *IEEE Signal Processing Letters* 7, 7 (2000), 179–181.
- Bernhard E Riecke, Hans-Günther Nusseck, and Jörg Schulte-Pelkum. 2006. Selected technical and perceptual aspects of virtual reality displays. (2006).
- Liang Shi, Beichen Li, Changil Kim, Petr Kellnhofer, and Wojciech Matusik. 2021. Towards real-time photorealistic 3D holography with deep neural networks. *Nature* 591, 7849 (2021), 234–239.
- Atsushi Shiraki, Naoki Takada, Masashi Niwa, Yasuyuki Ichihashi, Tomoyoshi Shimobaba, Nobuyuki Masuda, Tomoyoshi Ito, P S Hilaire, S A Benton, M Lucente, M L Jepsen, J Kollin, H Yoshikawa, and J Underkoffler. 2009. *Simplified electroholographic color reconstruction system using graphics processing unit and liquid crystal display projector*. References and links. Technical Report. <http://www.opticsinfobase.org/oe/abstract.cfm?id=81092>
- JMP Van Waveren. 2016. The asynchronous time warp for virtual reality on consumer hardware. In *Proceedings of the 22nd ACM Conference on Virtual Reality Software and Technology*. 37–46.
- David R Walton, Koray Kavaklı, Rafael Kuffner Dos Anjos, David Swapp, Tim Weyrich, Hakan Urey, Anthony Steed, Tobias Ritschel, and Kaan Akşit. 2022. Metameric Variifocal Holograms. In *2022 IEEE Conference on Virtual Reality and 3D User Interfaces (VR)*. IEEE, 746–755.
- Brian A Wandell. 1995. *Foundations of vision*. Sinauer Associates.
- Gaolei Xue, Juan Liu, Xin Li, Jia Jia, Zhao Zhang, Bin Hu, and Yongtian Wang. 2014. Multiplexing encoding method for full-color dynamic 3D holographic display. *Opt. Express* 22, 15 (Jul 2014), 18473–18482. <https://doi.org/10.1364/OE.22.018473>
- Daeho Yang, Wontaek Seo, Hyeonsung Yu, Sun Il Kim, Bongsu Shin, Chang-Kun Lee, Seokil Moon, Jungkwuen An, Jong-Young Hong, Geeyoung Sung, et al. 2022. Diffraction-engineered holography: Beyond the depth representation limit of holographic displays. *Nature Communications* 13, 1 (2022), 1–11.
- Lei Yang, Jun Xia, Chenliang Chang, Xiaobing Zhang, Zhiming Yang, and Jianhong Chen. 2015. Nonlinear dynamic phase response calibration by digital holographic microscopy. *Applied optics* 54, 25 (2015), 7799–7806.
- Xin Yang, Ping Song, HongBo Zhang, and Qiong-Hua Wang. 2019. Full-color computer-generated holographic near-eye display based on white light illumination. *Optics Express* 27, 26 (2019), 38236–38249.
- Fahri Yaraş, Hoonjong Kang, and Levent Onural. 2009. *Real-time phase-only color holographic video display system using LED illumination*. Technical Report.

- Kun Yin, En Lin Hsiang, Junyu Zou, Yannanqi Li, Zhiyong Yang, Qian Yang, Po Cheng Lai, Chih Lung Lin, and Shin Tsion Wu. 2022. Advanced liquid crystal devices for augmented reality and virtual reality displays: principles and applications. *Light: Science and Applications* 11, 1 (2022). <https://doi.org/10.1038/s41377-022-00851-3>
- Jingzhao Zhang, Nicolas Pégard, Jingshan Zhong, Hillel Adesnik, and Laura Waller. 2017. 3D computer-generated holography by non-convex optimization. *Optica* 4, 10 (2017), 1306–1313.
- Zichen Zhang, Zheng You, and Daping Chu. 2014. Fundamentals of phase-only liquid crystal on silicon (LCOS) devices. *Light: Science & Applications* 3, 10 (2014), e213–e213.

Supplementary Material – Simultaneous Color Holography

S1 ADDITIONAL IMPLEMENTATION DETAILS

Spatial Light Modulator. For all simulations, a spatial light modulator (SLM) with 1920×1080 pixels and a pixel size of $8 \mu\text{m} \times 8 \mu\text{m}$ is used. The phase ranges of the red, green, and blue channels are 2.4π , 5.9π , and 7.4π , respectively, unless otherwise noted. These values were experimentally calibrated for the Holoeye Pluto-2.1-Vis-016 SLM. The propagation distance of all simulated holograms is 100 mm unless otherwise noted.

Modified High Order Angular Spectrum Method (HOASM). We implement a modified version of the High Order Angular Spectrum Method (HOASM) as described by Gopakumar et al. [2021]. Instead of propagating the zero- and first-order together, we propagate them separately. The zero-order is propagated by performing the traditional angular spectrum method (ASM). To propagate the first-order, we pattern the zero-padded Fourier transform of the complex field to be propagated into a 3×3 grid. The center Fourier transform of the grid is then zeroed out. The Fourier representation of the first-order is then weighted with a sinc function and propagated to the sensor plane using ASM. The field is then down-sampled and cropped. The complex fields of the zero- and first-orders are then split into real and imaginary parts and stacked before being fed into a U-Net. The U-Net consists of 4 downsampling layers, the number of channels increases from 4 to 32 during the first downsampling layer and doubles in each of the next 3 downsampling layers until there are 256 channels. Four upsampling layers are then applied, producing a single-channel output representing the intensity of the propagated wavefront.

Camera Space to SLM Space Homography. To perform either offline or active camera-in-the-loop optimization, the captured wavefront and SLM must be in the same space. This requires a transform and downsampling of the captured image to place it in the same coordinate system as the SLM pattern used to generate it. We opt to use an affine transform to perform this mapping. The affine transform is calculated as follows: First, an SLM pattern is calculated that produces a grid of dots. The dots are then detected on the sensor, and their centers are estimated in camera space coordinates. The centers of the dots are known in SLM space since the target image containing the dots is in SLM space for optimization. Finally, Python’s OpenCV package is used to produce the affine transform matrix that maps the captured dots to the SLM coordinate space. A unique homography is calculated for each depth location and color channel.

Source Power Optimization. Correctly setting the power of each color channel of the SLED for a given hologram is an important step to achieving good color fidelity. To achieve this, we use an active camera-in-the-loop based approach to optimize the power of the color channels. First, the power of the source is set to an arbitrary value less than 100% across all three color channels. A baseline reference image is captured, debayered, and mapped to the SLM space. Three learnable weighting parameters, one for each color channel, are initialized to unity and applied to the captured reference image. These weighting parameters serve as a proxy to optimizing the source power. An iterative process is then undertaken, where an image is captured on the camera, debayered, and mapped to the SLM space. The loss between this image and the target image is calculated, and then backpropagated using the computational graph of the weighting parameters applied to the reference image. The initial source power is then multiplied by the updated weighting parameters, and a new image is captured, restarting the iterative loop. This is done until the color weighting parameters have converged, usually taking between 15-30 iterations. If the process fails to converge or the initial source power multiplied by the weighting function becomes greater than 100%, the exposure time is increased, and the source power optimization is restarted.

Although we use camera feedback in this process, we note that the information needed for source power optimization is contained in the color balance of the image itself. We believe this step could be replaced with a precomputed source power that’s dependent on the image content.

S2 ACTIVE CAMERA-IN-THE-LOOP (CiTL)

Active CiTL [Peng et al. 2020] is a special case of camera-calibrated models in which an image is displayed on the SLM, and camera captures are used to improve that particular image using the difference between the experimental capture and target image. While active CiTL is incompatible for real time displays, it does provide a useful proof of achievable hologram quality since. Consequently, we implemented active CiTL for our system as follows.

First, an SLM pattern is optimized using our learned simulation model and the computational graph is retained. This SLM pattern is then displayed and the resulting hologram is captured. A homography is applied to the captured hologram for each color channel to map it from camera space to simulation space. Our perceptual loss function is applied to the remapped captured hologram and target image. Backpropagation is performed using a computational graph saved during the forward pass, but the experimentally captured hologram is used in the loss function (instead of the simulated model output). This is the first time to our knowledge that active CiTL has been combined with a deep component to the forward model. Figure S1 shows reduced noise and improved color fidelity for holograms generated with active CiTL. Since active CiTL uses the difference between the experimental capture and the target, the alignment between the two must be precise. We find that improved alignment using a piecewise affine homography, rather than a global affine homography, dramatically improves color fidelity. A comparison of this case is shown in Figure S2.



Fig. S1. Active camera-in-the-Loop (CiTL) reduces noise and improves color fidelity. The first column of this image depicts experimentally captured color holograms. The second columns shows images that were iteratively improved with a camera in the system using the active CiTL algorithm of Peng et al. [2020].

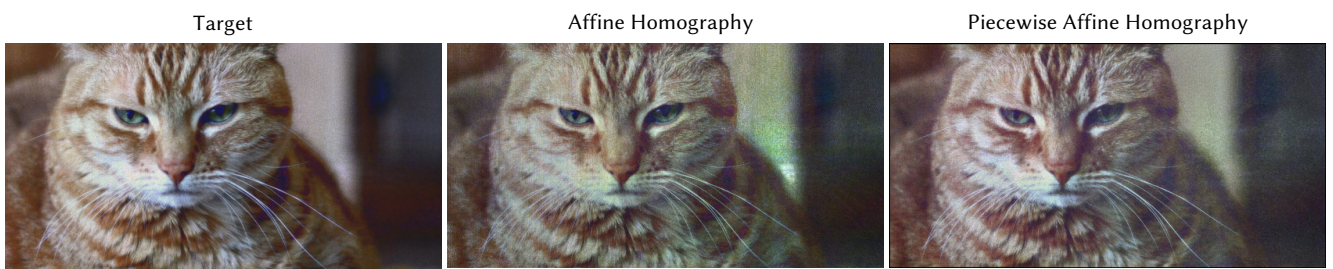


Fig. S2. Piecewise affine homography improves color fidelity for active CiTL. The first column shows the target image. The second column shows the experimentally captured hologram optimized using active CiTL with a global affine homography. The third column depicts active CiTL with a piecewise affine homography, which reduces color artifacts and noise due to better alignment during optimization. Cat source image by Chris Erwin (CC-BY-2.0).

S3 ADDITIONAL EXPERIMENTAL RESULTS AND FAILURE CASES

Figure S3 depicts additional captured results, which are intended to showcase a wider variety of scenes and include failure cases of our method. Our method has the most difficulty when the target has large, flat areas (i.e. textureless) of saturated color. Textureless targets lack high frequency information that can be leveraged by our loss function, leading to substantial artifacts such as color non-uniformity and ringing. These artifacts are particularly apparent in the image of colored bars in Fig. S3. Highly saturated images or “unnatural” images (like the colored bars) often fail due to disparate color channels, resulting in a single SLM pattern having to produce three holograms at the same plane with substantially different structures. In contrast, natural images typically have similarly structured color channels.

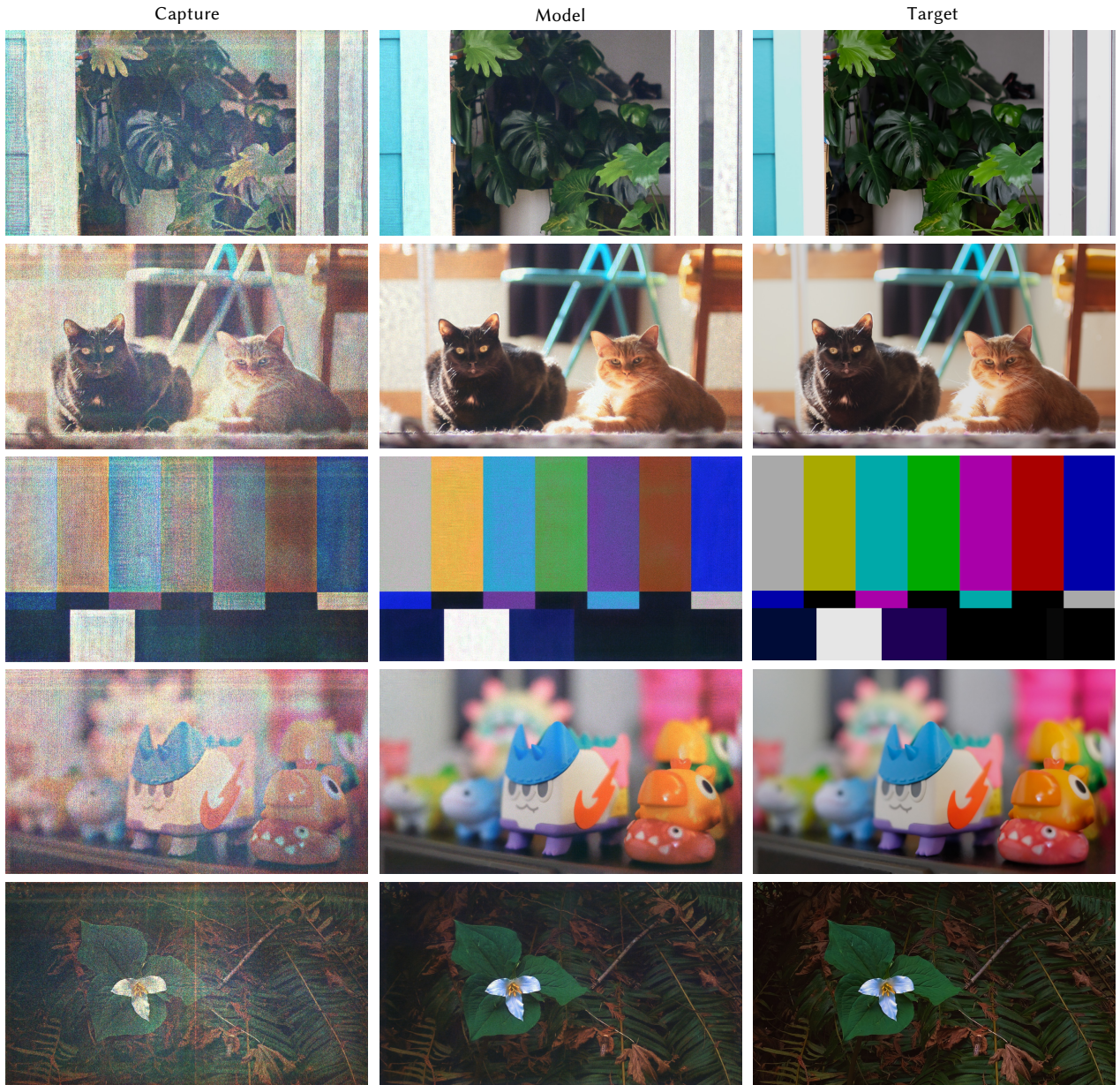


Fig. S3. Additional simultaneous color holograms captured in experiment. The first column depicts holograms captured in experiment. The second column shows the simulation output. The third column depicts the target image. Although our system performs well on most natural scenes, unnatural images such as the bars in the center row are more challenging for our algorithm.

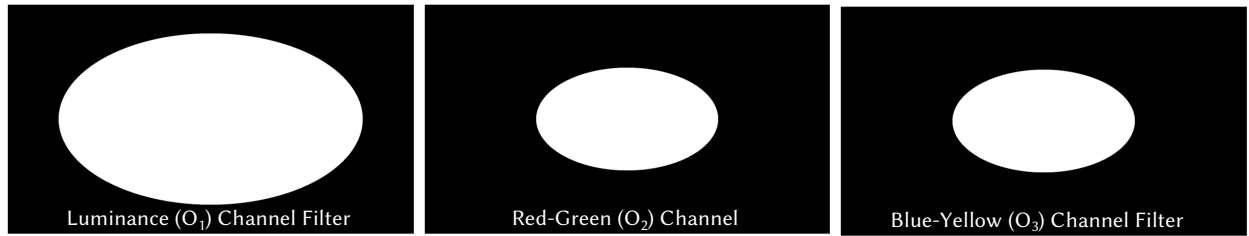


Fig. S4. Perceptual loss function filters in Fourier opponent color space. The white areas of the filters pictured represents the pass band of the filter. The luminance channel has a filter width of 75% of Fourier space. Both chrominance channels (Red-Green, Blue-Yellow) have filter widths of 45% of Fourier space.

S4 ADDITIONAL PERCEPTUAL LOSS FUNCTION DETAILS

The filter sizes for our perceptual loss function were chosen heuristically, such that no visible change was noticeable between the target image and the target image with the perceptual filter applied. These filter sizes were kept constant regardless of the scene being optimized. These filters can be viewed in Fig. S4 To test the effectiveness of our perceptual loss function, we applied it to a personally captured dataset of 294 images. For each target image, an SLM pattern was optimized using both the traditional RGB loss function and our perceptual loss function. The resulting hologram was then captured, and the perceptual filter was applied. The PSNR, SSIM, and NMSE were calculated for the filtered simulated holograms and the perceptually filtered target image. The average metrics over the entire dataset are provided in Table S1.

	PSNR	SSIM	NMSE
RGB Loss Function	20.11	0.603	0.010
Perceptual Loss Function	26.58	0.869	0.003

Table S1. A comparison of the average PSNR, SSIM, and NMSE for holograms optimized with the traditional RGB loss function and perceptual loss function. The metrics were calculated between the perceptually filtered simulated holograms and the perceptually filtered target. The data set used was a personally captured set of 294 images of natural scenes.

S5 THE EFFECT OF BIT DEPTH ON HOLOGRAM QUALITY

The effect of quantization on hologram quality is an important consideration when choosing an extended phase SLM. We define the effective bit depth as the number of bits contained in a 2π interval of the extended range. For example, the effective bit depth of an 8-bit SLM with a phase range of 8π is 6 bits as each 2π interval contains 64 discrete samples i.e. 6 bits. To determine the minimum bit depth required for adequate image quality, we simulated holograms using an SLM with a 2π phase range and bit depths from 2 bits to 8-bits. Simulations are done by optimizing the hologram with gradient descent, then quantizing to the target bit depth. A significant drop off in both PSNR and SSIM was observed between 5 and 6 bits, as depicted in Fig. S5. This suggests that the minimum effective bit depth required for an extended phase SLM is 6 bits. Since most commercially available SLMs are 8 bits, this suggests that the maximum phase range in any channel should be 8π , which aligns well with the SLM used in our experiments (maximum phase range of 7.4π in the blue channel).

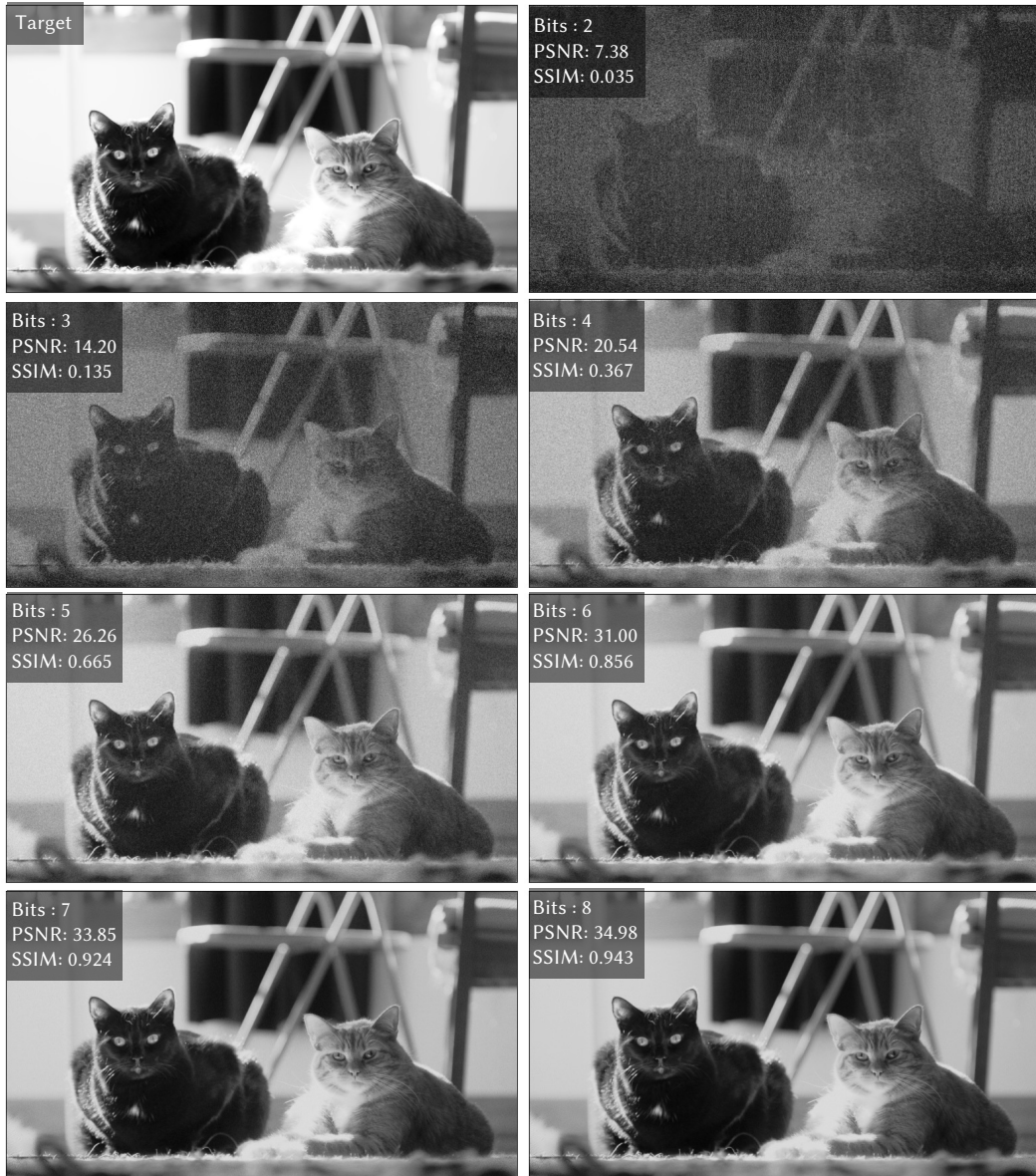


Fig. S5. **An analysis of SLM bit depth on hologram quality in simulation** We simulate holograms using SLMs of 2 to 8 bits. The target image is pictured in the top left of the figure. One should note the rapidly increasing drop off in both PSNR and SSIM between 5 and 6 bits.

S6 BIT AND DEPTH DIVISION IMPLEMENTATION DETAILS AND ANALYSIS

In this section we provide our implementation details of bit and depth division holography. Additionally, we analyze the methods for SLMs of various phase ranges. We implement bit division largely as laid out by Jesacher et al. [2014]. First we calculated the three color channels SLM patterns using a modified Gerchberg-Saxton approach assuming a 2π phase range in each color channel. Instead of using the Fourier transform for propagation as in Jesacher et al. [2014], we use ASM match our other results. This is run until convergence, and 3 unique SLM patterns are produced. These SLM patterns are then combined via an optimization problem as described by [Jesacher et al. 2014]. We then used the combined SLM pattern to simulate a color hologram at the sensor plane.

We choose to implement the depth division method using gradient descent-based optimization rather than a modified Gerchberg-Saxton (GS) algorithm for multiplane holograms originally proposed by Makowski et al. [2010, 2008] for depth division holography. Since we use gradient descent in our approach, we determined this was a fairer comparison. In our implementation the SLM pattern is first converted to a complex field. The complex field is then propagated to $z = 68$ mm, 80 mm, 100 mm using the ASM kernel for the red color channel. These correspond to the replica planes. The intensity of the fields are then calculated at each target plane and compared to the blue, green, and red channels, respectively, using an L2 loss function. Backpropagation is then used to calculate the gradients of the loss function with respect the SLM voltage values and then update these voltages.

We implement both the bit and depth division holography methods for 3 simulated SLMs. The first SLM has a uniform 2π phase range in each color channel. This phase range is optimal for depth division, but performs the worst of the simulated SLMs for bit division, demonstrating how bit division relies on extended SLM phase range. The next simulated SLM is an arbitrary standard SLM i.e. not extended phase. We model this SLM to have 2π phase range in red, 2.7π in green, and 3.4π in blue. The simulated holograms increase in quality from the 2π SLM for the bit division method, but decrease in quality for depth division. Finally we simulate the Holoeye Pluto SLM used in our experimental setup. This SLM has a 2.4π phase range in red, 5.9π phase range in green, and 7.4π phase range in blue. The results for depth division continue to degrade with this SLM, since the depth division algorithm does not take into account the wavelength-dependent response of the SLM. The results improve for bit division with the additional extended phase. This suggests that that phase diversity across channels provides the best performance for bit division holography, while phase uniformity across channels provides the best performance for depth division holography. The results of the outlined experiment can be found in Figs. S6 and S7.

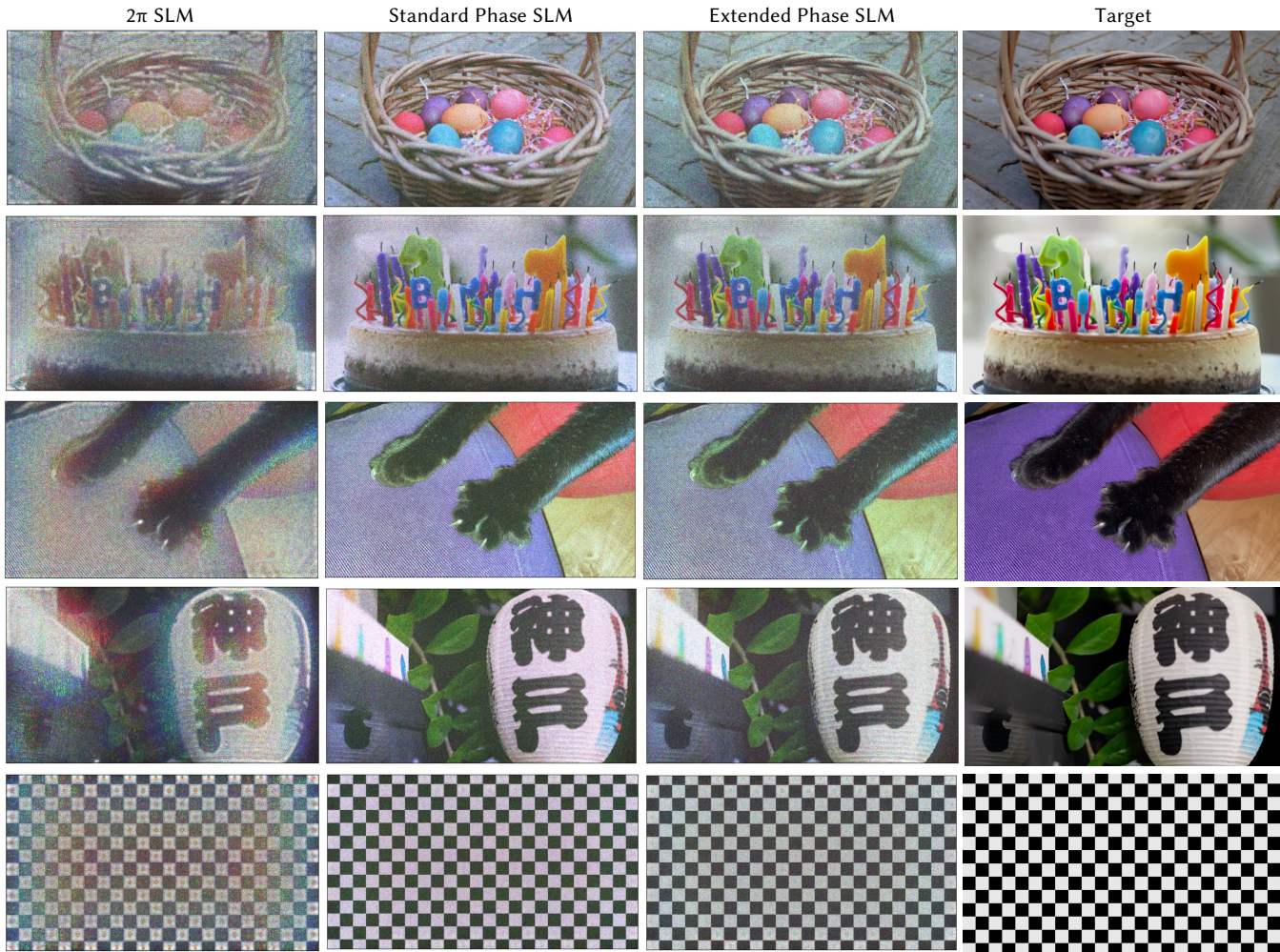


Fig. S6. **SLM phase range affects hologram quality for bit division holography.** Bit division takes advantage of the extended phase range of the SLM, so does not perform well with an SLM with only 2π phase range per channel (left column). With a “standard” SLM with realistic wavelength dependence to the phase, bit division performs better. It works best with the extended phase range of the simulated Holoeye Pluto that we use for our experiments.

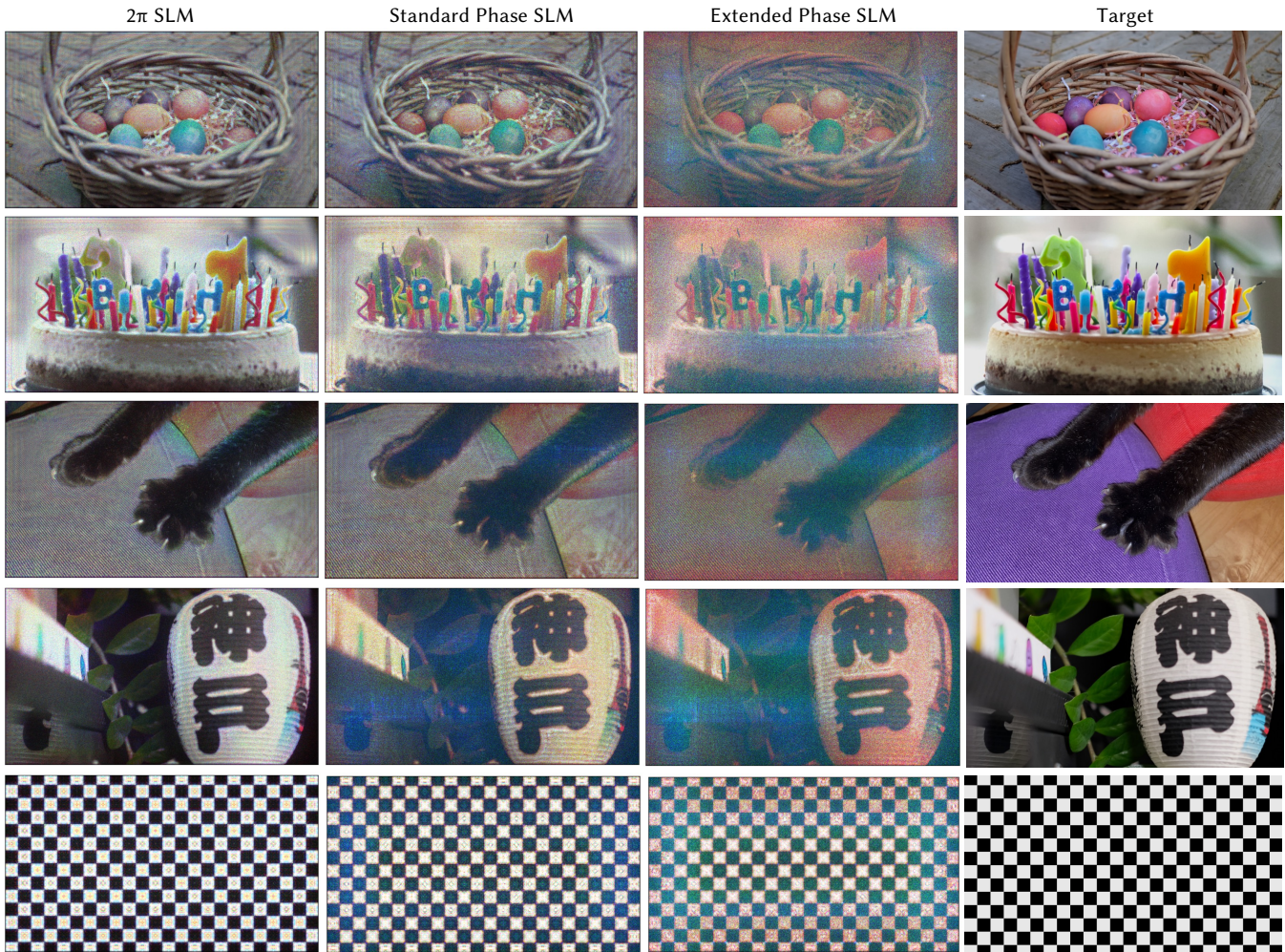


Fig. S7. SLM phase range affects hologram quality for depth division holography. The depth division approach assumes no wavelength dependence of the SLM, which is simulated in the first column. With standard SLM with 2π phase in red and realistic wavelength dependence (second column) the results are slightly degraded due to inaccurate modeling of the SLM response. Finally, with the extended phase range of the simulated Holoeye Pluto SLM, the results show significant color artifacts and noise.